Please cite this article in press as: Rahjouei et al., MAD2L2 Promotes Open Chromatin in Embryonic Stem Cells and Derepresses the *Dppa3* Locus, Stem Cell Reports (2017), http://dx.doi.org/10.1016/j.stemcr.2017.02.011

Stem Cell Reports
Report

ISSCR

OPEN ACCESS

MAD2L2 Promotes Open Chromatin in Embryonic Stem Cells and Derepresses the *Dppa3* Locus

Ali Rahjouei,[1,2] Mehdi Pirouz,[1,4] Michela Di Virgilio,[2] Dirk Kamin,[3] and Michael Kessel[1,*]
[1]RG Developmental Biology, Max Planck Institute for Biophysical Chemistry, Am Fassberg, 37077 Göttingen, Germany
[2]DNA Repair and Maintenance of Genome Stability, Max-Delbruck Center for Molecular Medicine, 13125 Berlin-Buch, Germany
[3]Department NanoBiophotonics, Max Planck Institute for Biophysical Chemistry, Am Fassberg, 37077 Göttingen, Germany
[4]Present address: Stem Cell Program, Boston Children's Hospital and Department of Biological Chemistry and Molecular Pharmacology, Harvard Medical School, Boston, MA 02115, USA
*Correspondence: mkessel1@gwdg.de
http://dx.doi.org/10.1016/j.stemcr.2017.02.011

SUMMARY

The chromatin of naive embryonic stem cells (ESCs) has a largely open configuration, as evident by the lack of condensed heterochromatin and the hypomethylation of DNA. Several molecular mechanisms promoting this constellation were previously identified. Here we present evidence for an important epigenetic function of MAD2L2, a protein originally known for its role in DNA damage repair, and for its requirement in germ cell development. We demonstrate using super-resolution microscopy that numerous MAD2L2 microfoci are exclusively associated with euchromatin, similar to other factors of the DNA damage response. In the absence of MAD2L2 the amount of heterochromatin demarcated by H3K9me2 was significantly increased. Among the most strongly suppressed genes was *Dppa3*, an ESC- and germ-cell-specific gene regulating DNA methylation. In *Mad2l2*-deficient ESCs 5-methylcytosine levels were globally increased, while several imprinted genes became hypomethylated and transcriptionally activated. Our results emphasize the important function of MAD2L2 for the open chromatin configuration of ESCs.

INTRODUCTION

Open chromatin is a global, constitutive feature of naive embryonic stem cells (ESCs), which are characterized by low levels of repressive histones and DNA methylation (Gaspar-Maia et al., 2011; Meshorer and Misteli, 2006). Diverse factors are required to maintain ESC chromatin in a decondensed state. They are important to stabilize pluripotency and to maintain the potential for self-renewal and differentiation. DPPA3 (also called PGC7 or Stella) is one of the factors known to modulate epigenetic processes in both embryonic and germ cell development (Payer et al., 2003). It is a highly specific, maternal effect gene required for early embryonic cells and primordial germ cells (PGCs), and demarcates naive versus primed pluripotency (Hayashi et al., 2008; Ohinata et al., 2008). Heterogeneous expression of DPPA3 was detected in ESC populations growing in Lif/serum as well as LIF/2i medium (Hayashi et al., 2008; Singer et al., 2014). DPPA3 heterogeneity was concluded to result from a combination of low burst frequencies and large burst sizes (Singer et al., 2014). DPPA3 is known to be involved in the maintenance of the low level of DNA methylation typical for early embryonic cells as well as ESCs (Hayashi et al., 2008). At the same time, it protects imprinted loci against demethylation (Nakamura et al., 2007). DPPA3 is required for the generation of fully reprogrammed pluripotent stem cells, in particular for the erasure of the epigenetic memory encoded in the DNA methylation pattern (Xu et al., 2015b).

Both ESCs and PGCs, the two cell types characterized by the expression of DPPA3, require the MAD2L2 protein for the proper establishment of their epigenetic status (Pirouz et al., 2013, 2015). In the absence of Mad2L2 PGCs do not reprogram toward a more flexible chromatin configuration after their induction, and ESCs are not able to propagate their typical open chromatin, which is necessary for stable pluripotency.

MAD2L2 (also called REV7 or MAD2B) was originally identified by its function in DNA repair, playing an accessory role in translesion DNA repair and an inhibitory role in the resection of 5′ ends after DNA double-strand breaks and at unprotected telomeres (Boersma et al., 2015; Xu et al., 2015a). As a downstream component of the DNA damage response pathway, MAD2L2 promotes non-homologous end joining versus homologous recombination. The role of MAD2L2 in DNA repair, ESC development, and PGC development is tightly connected to the epigenetic status of the respective cells. To investigate the relationship between MAD2L2 and the formation of open chromatin we compared wild-type and *Mad2l2*-deficient ESCs, employing super-resolution microscopy, transcriptome sequencing, methylome sequencing, and chromatin immunoprecipitation sequencing (ChIP-seq) analysis. We identified *Dppa3* as a downstream target of MAD2L2, and derived a model explaining the epigenetic effects of MAD2L2.

Please cite this article in press as: Rahjouei et al., MAD2L2 Promotes Open Chromatin in Embryonic Stem Cells and Derepresses the *Dppa3* Locus, Stem Cell Reports (2017), http://dx.doi.org/10.1016/j.stemcr.2017.02.011

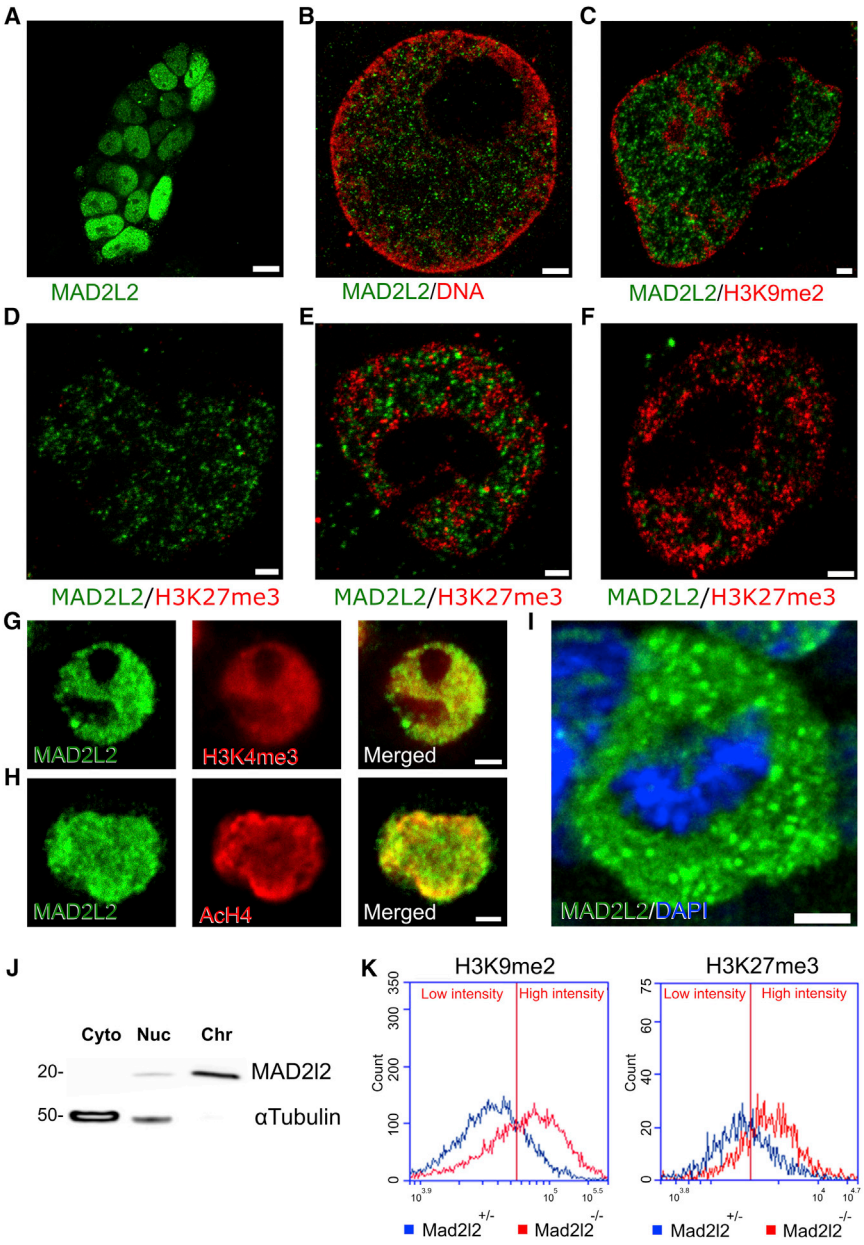

Figure 1. MADL2 Localization in Relation to Open and Closed Chromatin of ESCs

(A) Confocal microscopy of a colony with MAD2L2-positive and -negative ESCs.

(B–F) STED microscopy of ESC sections (B, 50 nm; C–F, 80 nm) were analyzed by immunocytochemistry for (B) DNA, (C) H3K9me2, and (D–F) H3K27me3.

(G) MAD2L2 expression in ESCs overlapped with euchromatin as identified by H3K4me2 (G) and AcH4 (H).

(I) ESC with condensed chromosomes in the metaphase of the cell cycle. The cell was stained for DNA (DAPI, blue), and MAD2l2 (red), and analyzed by confocal microscopy. See also Figures S1 and S2.

(J) Fractionation of ESCs revealed that virtually the complete amount of MAD2L2 protein was in the chromatin fraction (Chr), and not in the cytoplasm (Cyto) or the nuclear fraction remaining after chromatin separation (Nuc).

(K) The numbers of ESCs expressing high levels of H3K9me2 or H3K27me3 were significantly increased in the absence of MAD2L2.

All observations in were confirmed with three experimental replicates. Scale bars represent 10 μm (A), 0.86 μm (B–F), 4 μm (G and H), and 10 μm (I).

RESULTS

Heterogeneous Expression of MAD2L2 in ESCs

ESCs are known to express variable levels of specific RNAs and/or proteins, depending among other factors on growth conditions. This indicates a highly dynamic regulation of gene expression and reflects a metastable equilibrium between distinct cellular states. We characterized the MAD2L2 protein in wild-type ESCs and compared the dynamics with classical ESC markers. Individual cells of a colony expressed significantly different levels of MAD2L2 (Figure 1A and Movie S1), either very high (4.8% out of 1,000 evaluated, cells from five different fields), high (72%), or low (23.2%), resembling the heterogeneity observed for DPPA3 expression (Figure 3A) (Hayashi et al., 2008). In contrast, both MAD2L2-positive and -negative ESCs expressed Oct4 (Figure S1A). The differentiation of ESCs into epiblast-like cells (EpiLC) represents the transition from naive to primed pluripotency (Hayashi et al., 2011). This was accompanied by a drastic downregulation of the MAD2L2 protein (Figure S1B) and *Dppa3* mRNA (Figure 3C). Together, these observations suggest a dynamic fluctuation from a state of naive pluripotency demarcated by *Mad2l2* and *Dppa3* expression to a primed state with both markers

off. EpiLCs can be further converted to unipotent PGC-like cells (PGCLCs), close in vitro equivalents of PGCs, on embryonic day 9 (Hayashi et al., 2011). PGCLCs represent exactly the developmental stage at which a crucial function of MAD2L2 was previously demonstrated (Pirouz et al., 2013). High expression levels of both MAD2L2 and DPPA3 are typical for germ cells including PGCLCs, and for naive ESCs (Figures S2A and 3C).

Association of MAD2L2 with Open Chromatin/Euchromatin

In ESCs the MAD2L2 protein was associated with the chromatin fraction; however, it did not decorate condensed, mitotic chromosomes (Figures 1I and 1J). Super-resolution microscopy revealed that it was distributed in microfoci, not overlapping with the DNA-enriched heterochromatin near the nuclear lamina and around the nucleolus, as identified by H3K9me2 (Figures 1B and 1C) (Willig et al., 2006). High levels of MAD2L2 protein were found in many ESCs of a colony in regions separate from transcriptionally inactive chromatin, as identified by H3K27me3 (Figures 1E and 1F). H3K27me3 accumulated in more central areas of ESC nuclei, compared with the peripheral localization of H3K9me2 (Figures 1C and 1E). ESC colonies always additionally contained cells with either predominantly MAD2L2 or predominantly H3K27me3, but not both, proteins (Figures 1D and 1F). More precisely, 70.6% of wild-type ESCs (out of 1,141 evaluated cells, from four fields) predominantly expressed MAD2L2 in the absence of H3K27me3, 23.6% had a non-overlapping expression of both MAD2L2 and H3K27me3, and 5.7% predominantly expressed H3K27me3 in the absence of MAD2L2. These numbers reflect the highly dynamic chromatin status in ESCs. Line scan histogram profiles through single nuclei demonstrated that MAD2L2 did not co-localize with compacted DNA and the heterochromatin markers H3K9me2, H3K27me3, and HP1α (Figure S1C). In contrast to its exclusion from heterochromatin, MAD2L2 co-localized completely with the euchromatin identified by H3K4me3 and AcH4, which are the dominant histone modifications in ESCs growing in LIF/2i (Figures 1G and 1H).

Like ESCs, PGCLCs also express significant levels of MAD2L2 (Figure S2A). To investigate whether MAD2L2 is instrumental for the balance between open and closed chromatin, we analyzed *Mad2l2*-deficient ESCs and PGCLCs. Mutant ESCs had an increased amount of heterochromatin, as indicated by the global levels of H3K9me2 and H3K27me3, and by a significantly increased number of cells with high levels of H3K9me2 and H3K27me3 (Figure 1K). The differentiation of ESCs via EpiLCs into PGCLCs was normally accompanied by the re-induction of the *Oct4*-GFP transgene and by a loss of the high levels of H3K9me2 typical for EpiLCs (Figure S2B). However, *Mad2l2*-deficient PGCLCs maintained high levels of H3K9me2 and were not able to reprogram toward H3K27me3 (Figure S2C). This resembled the initial induction of *Mad2l2*-deficient PGCs and their defective epigenetic reprogramming observed in vivo (Pirouz et al., 2013). Taken together, we found a correlation between the presence of Mad2l2 and an open chromatin configuration, as is typical for naive pluripotency and germ cells after their epigenetic reprogramming. In the absence of *Mad2l2*, ESCs accumulated heterochromatin and lost their naive pluripotency. *Mad2l2*-deficient PGCLCs were locked in their stably repressed chromatin configuration.

Focus Formation in ESCs and Mitomycin-Treated MEFs

Not only MAD2L2, but also other DNA damage response factors accumulated in microfoci in the nuclei of ESCs, although there was no prior induction of DNA damage (Figures 2A–2C) (Banath et al., 2009; Turinetto et al., 2012). Phosphorylation of histone H2AX and accumulation γH2AX foci around the sites of DNA breaks are usually an immediate-early response to DNA damage. In ESCs they were mainly localized, but not necessarily restricted, to areas of low DNA density (Figure 2A). Foci of the E3 ligase RNF168 and of the large adaptor protein 53BP1 were restricted to open chromatin, and their sizes were smaller, quite similar to the MAD2L2 microfoci (Figures 2B and 2C).

ESCs were co-cultured on feeder layers consisting of mitomycin-treated (i.e., DNA damaged) murine embryonic fibroblasts (mMEFs). This allowed a side-by-side comparison of foci formed in response to DNA damage with ESC foci (Figures 2D–2F). Mitomycin C-induced MAD2L2 foci varied widely in size (1–3.5 μm) in the intensity of staining for MAD2L2 and in numbers per nucleus, clearly due to the random nature of DNA damage induction. Focus sizes in ESCs were generally smaller (approximately 0.2–0.3 μm) and the numbers per cell were drastically higher, being homogeneously distributed throughout the open chromatin regions of ESC nuclei, separate from DAPI-stained, condensed heterochromatin (Figures 2D–2F). Thus, the parallel scanning of ESCs and mMEFs revealed an inverse relationship between the level of MAD2L2 and the presence of DAPI-stained heterochromatin. It also demonstrated the principal differences underlying focus formation in response to DNA damage and in ESCs.

Repression of the *Dppa3* Locus in the Absence of MAD2L2

We had previously compared the transcriptomes of *Mad2l2*-deficient and wild-type ESCs, and identified major transcriptional changes (Pirouz et al., 2013). A re-evaluation of the transcriptome data (see Experimental Procedures) revealed that the fourth most significantly downregulated gene was *Dppa3* (Figure 3B). Downregulation of

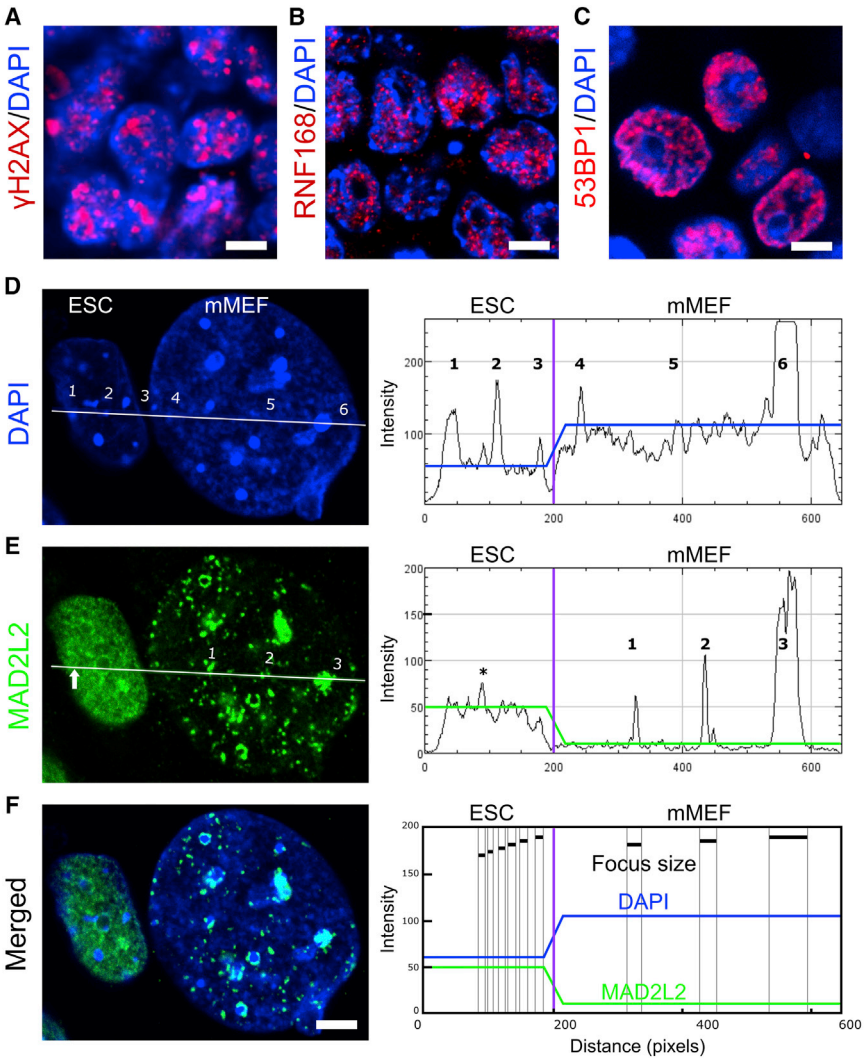

Figure 2. Microfoci of DNA Damage Response Factors in Wild-Type ESCs and Mitomycin-Treated MEFs

(A–C) γH2AX, RNF168, and 53BP1 microfoci in ESCs.

(D–F) Direct comparison of an ESC with a mMEF, which were scanned along the white line. The localization of proteins in comparison with DAPI was studied in at least 100 nuclei. (D) DAPI-intense DNA foci; the blue line compares average levels of DNA and numbers indicate condensed DNA foci. (E) MAD2L2 microfoci; the green line compares average levels of MAD2L2 protein, numbers indicate MAD2L2 foci, and white arrow points to the microfocus identified by an asterisk in the line scan histogram. (F) The merge of (D) and (E) compares directly DNA (DAPI) foci with the MAD2L2 foci. Black lines indicate the diameter of foci. Scale bars represent 10 μm (A–C) and 5 μm (F).

Dppa3 in the absence of MAD2L2 was confirmed by RT-PCR for ESCs, EpiLCs, and PGCLCs (Figure 3C), and for ESCs also by immunofluorescence (Figure 3A). We used the BVSC cell line to visualize *Dppa3* expression by fluorescence of the DPPA3-eCFP fusion protein. DPPA3-positive and -negative ESCs were sorted based on expression of the ECFP reporter, and qPCR confirmed a positive correlation between *Dppa3* and *Mad2l2* levels. When sorted ESCs with a low level of DPPA3 were recultured in LIF/2i medium, 7% of the cells had upregulated the expression of *Dppa3*, suggesting that *Mad2l2* expression also could recover (Figures S3A–S3C).

ChIP-seq analysis of the *Dppa3* locus revealed that its transcriptional repression in *Mad2l2*-deficient ESCs was associated with the deposition of the repressive histone H3K9me2 in two positions upstream of the transcriptional start site (Figure 3D). The expression of *Dppa3* could be rescued by the introduction of a vector encoding a MAD2L2-GFP fusion protein into Mad2l2-deficient ESCs (Figure 3E). In this experiment the reactivation of the *Dppa3* gene occurred in the absence of DPPA3 protein. Thus, the initial effect of MAD2L2 was exerted independently of the epigenetic function(s) of DPPA3. Once derepressed, the *Dppa3* locus could be transcribed in ESCs, probably under control of the core pluripotency factor PRDM14, which was previously shown to be necessary for *Dppa3* expression in PGCLCs (Magnusdottir et al., 2013). Remarkably, ESC colonies overexpressing GFP-MAD2L2 expressed DPPA3 as visualized by a *Dppa3-eCFP* transgene uniformly without an indication for heterogeneity (Figure 3F).

Global Increase of DNA Methylation, and Specific Demethylation of Imprinted Loci in *Mad2l2*-Deficient ESCs

We measured a significant increase of the global levels of 5-methylcytosine in *Mad2l2*-deficient ESCs compared

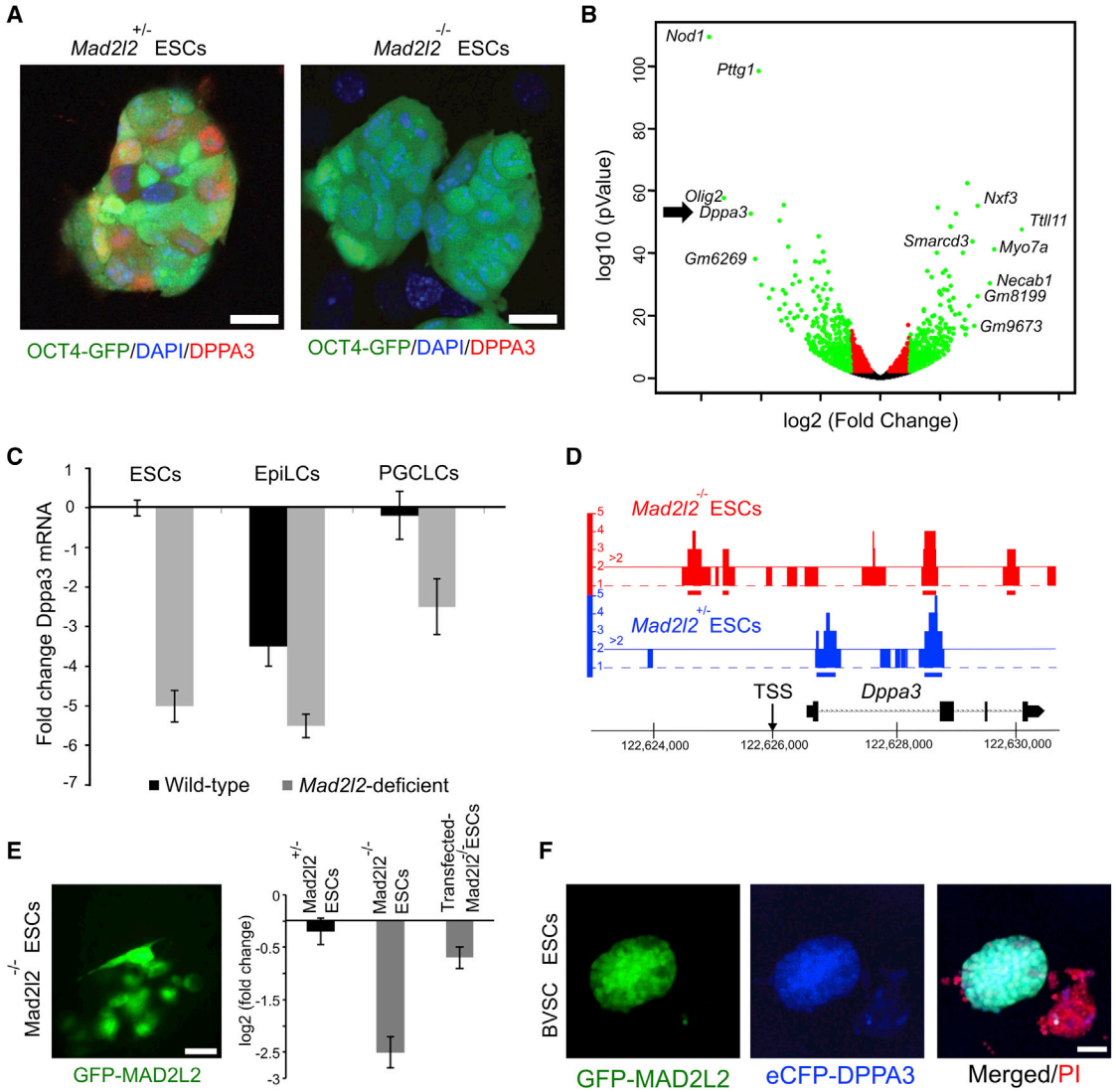

Figure 3. *Dppa3* as a Target of MAD2L2

(A) Levels of DPPA3 protein are heterogeneous in a colony of wild-type ESCs (Hayashi et al., 2008), while no DPPA3 is detected in *Mad2l2*-deficient ESCs.

(B) Comparison of transcriptomes from wild-type and *Mad2l2*-deficient ESCs. The volcano plot displays downregulated genes on the left and upregulated genes on the right. Black dots refer to insignificant changes, and red and green dots to statistically significant up- or downregulated genes, with a $\log_2$ fold-change cutoff. The arrow points to *Dppa3* as the fourth most strongly decreased gene.

(C) *Dppa3* mRNA levels in ESCs, EpiLCs, and PGCLCs, in the presence (black) or absence (gray) of *Mad2l2*. SDs were calculated based on three experimental replicates.

(D) Deposition of H3K9me2 is significantly increased in two specific positions upstream of the Dppa3 transcription start site (TSS) in Mad2l2-deficient ESCs. The TSS was taken from the Database of Transcriptional Start Sites (DBTSS, http://dbtss.hgc.jp). Three experimental replicates were performed.

(E) RT-PCR analysis demonstrated the downregulation of Dppa3 expression in *Mad2l2*-deficient ESCs. Expression of *Dppa3* mRNA was efficiently rescued after transfection with an expression vector encoding a GFP-DPPA3 fusion protein. SDs were calculated based on three experimental replicates.

(F) BVSC ESCs (Ohinata et al., 2008) were transfected with *GFP-Mad2l2*, resulting in either completely GFP-positive or GFP-negative colonies. *Dppa3* expression was visualized by the blue fluorescence of ECFP protein originating from the transgene stably integrated in the endogenous *Dppa3* locus. Note the high, uniform expression of ECFP-DPPA3 in the Mad2l2-overexpressing colony, whereas the untransfected colony displayed normal heterogeneity. Three experimental replicates were performed.

Scale bars represent 25 μm (A), 25 μm (E), and 50 μm (F). See also Figure S3.

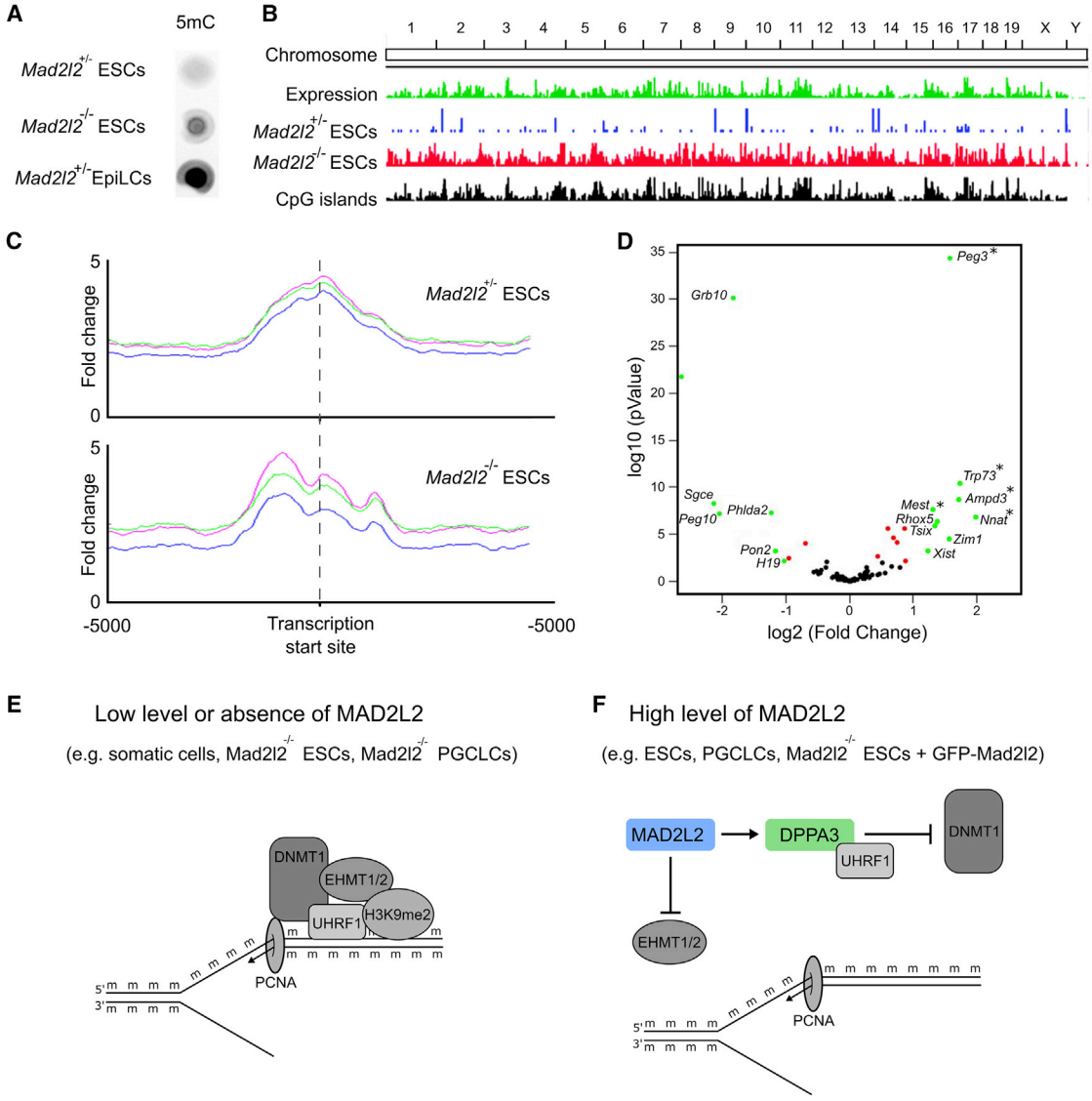

Figure 4. MAD2L2 Regulates DNA Methylation via DPPA3

(A) The low level of 5mC detected by dot blots prepared from ESCs grown in LIF/2i conditions was significantly elevated in mutant ESCs, without, however, reaching the level detected in EpiLCs. This observation was confirmed with three experimental replicates.

(B) 5mC-containing DNA fragments were immunoprecipitated and sequenced. This analysis revealed a global increase of DNA methylation in *Mad2l2*-deficient ESCs at single-base resolution. Three experimental replicates were performed.

(C) The patterns of DNA methylation were significantly altered in the mutant ESCs. For instance, methylation around the transcription start site was distributed in a single peak in wild-type cells, whereas a three-peak pattern was observed in mutant ESCs. See also class III in Figure S4. Red, green, and blue curves represent the values from three experimental replicates.

(D) Direct comparison of RNA-seq data with the MeDIP data. The volcano plot compares expression of imprinted genes in *Mad2l2*-deficient ESCs with wild-type ESC; on the right are activated genes, on the left repressed genes. Black dots refer to insignificant changes, while red and green dots refer to significantly up- or downregulated genes with a $\log_2$ fold-change cutoff. Note that the top five genes (labeled with asterisks), which were both demethylated and transcriptionally activated in *Mad2l2*-deficient ESCs, are known imprinted genes.

(E and F) Model for the binding of methyltransferases and interacting proteins near the replication fork. (E) The replication fork in the presence of low MAD2L2 levels as seen, for example, in somatic cells, *Mad2l2*$^{-/-}$ ESCs, or *Mad2l2*$^{-/-}$ PGCLCs. In the absence of MAD2L2 and DPPA3, H3K9me2 can contribute to the recruitment of DNMT1, UHRF1, EHMT1, and EHMT2. Consequently, the methylation of DNA and

(legend continued on next page)

with wild-type cells, although the high level found in EpiLCs was not reached (Figure 4A). Analysis of DNA methylation by methylated DNA immunoprecipitation sequencing (MeDIP-seq) confirmed the observed global difference, and allowed the display of DNA methylation at a single-nucleotide resolution (Figure 4B). These data revealed substantial, genome-wide perturbations of methylation patterns. For example, they demonstrated the presence of three methylation peaks instead of one around transcriptional start sites in mutant ESCs (Figures 4C and S4). Noteworthy, however, is that the *Dppa3* gene and its upstream region remained largely unmethylated in both wild-type and mutant ESC. In early embryonic cells several genes maintain their methylation in a widely undermethylated epigenetic landscape, and consequently are transcriptionally repressed (Habibi et al., 2013). DPPA3 was previously shown to play a role in this imprinting of genes (Bortvin et al., 2004; Kang et al., 2013; Nakamura et al., 2007). To study this process in *Mad2l2*-deficient, and consequently *Dppa3*-repressing, ESCs, we compared the RNA-seq datasets with the MeDIP-seq data. A total of 221 genes were methylated in wild-type ESCs but were unmethylated and transcriptionally upregulated in the *Mad2l2*-deficient ESCs (Figure 4D). Of these, the top five (*Peg3*, *Trp73*, *Ampd3*, *Mest*, and *Nnat*) were known imprinted genes (http://www.geneimprint.com). Taken together, the perturbation of DNA methylation in *Mad2l2*$^{-/-}$ ESCs not only resulted in a general increase of methylation, but also affected imprinting through demethylation of specific loci. Although the *Mad2l2*-deficient ESCs were shown to be pluripotent and capable of contributing to chimeras (Pirouz et al., 2015), they were not classified as naively pluripotent cells with regard to the increased level of DNA methylation.

DISCUSSION

The absence of MAD2L2 in mutant ESCs corresponds with the low MAD2L2 levels observed in somatic cells (Figure 4E). Cells with a low level of MAD2L2 have in common that the inhibitory binding of MAD2L2 to EHMT1 and EHMT2 is reduced (Pirouz et al., 2013). Thus, histone H3 can be efficiently methylated on residue K9, and H3K9me2 can then form a docking place for further epigenetic regulators. DNA methyltransferase DNMT1 is recruited together with UHRF1 and EHMT2 at the replication fork, where it will also bind to proliferating cell nuclear antigen, and cooperatively to hemimethylated DNA (Esteve et al., 2006; Liu et al., 2013; Rothbart et al., 2012). Together, these and other interacting factors represent an assembly of both chromatin writers and readers, which maintain and establish a cell-specific chromatin configuration (Liu et al., 2013; Shinkai and Tachibana, 2011). Collectively, the low levels of MAD2L2 and DPPA3 correspond to high levels of repressive histone modifications, substantial DNA methylation, and thus a closed chromatin configuration. In contrast, MAD2l2 levels are high in wild-type ESCs and PGCLCs, downstream of a cascade resembling the DNA damage response pathway (Figures 1A–1I and S2A). In such cells MAD2L2 can directly bind to both EHMT1 and EHMT2, suppress EHMT2 expression, and thus inhibit histone H3K9 and DNA methylation (Pirouz et al., 2013). By antagonizing the formation of H3K9me2, MAD2L2 will derepress the *Dppa3* gene. DPPA3 can then displace DNMT1 from UHRF1 at the replication fork, so that the growing strand cannot be methylated (Figure 4F; Funaki et al., 2014). In any case, the combined presence of MAD2L2 and DPPA3 in ESCs correlates with their generally low levels of both DNA and histone H3K9 methylation, i.e., a generally open chromatin configuration. In conclusion, the global promotion of open chromatin, and the inhibition of heterochromatin in ESCs and germ cells (PGCLCs and PGCs) depend critically on MAD2L2. The local opening of chromatin observed around DNA breaks may involve MAD2L2 and a similar mechanism (Noon et al., 2010). It is conceivable that the major importance of MAD2L2 lies in its epigenetic functions, be it in a stem or germ cell context, or in response to DNA damage.

EXPERIMENTAL PROCEDURES

Cell Culture

Mad2l2-deficient ESCs carrying an *Oct4-GFP* allele (Pirouz et al., 2015), and BVSC ESCs, with an insertion of the CFP reading frame into the *Dppa3* locus (Ohinata et al., 2008) were cultured in LIF/2i medium (Ying et al., 2008). For PGCLC formation, ESCs were first differentiated for 2 days into EpiLCs in the presence of activin and fibroblast growth factor, and subsequently for 6 days in PGCLC differentiation medium as described by Hayashi et al. (2011). See Supplemental Experimental Procedures for further details.

Flow Cytometry

Three independent biological replicates of 10,000 cells each were read by an Accuri C6 cytometer (BD Biosciences). See Supplemental Experimental Procedures for further details.

histones could proceed in coordinated fashion by the methyltransferases DNMT1 or EHMT1/2. (F) The replication fork in the presence of high MAD2L2 levels as seen, for example, in wild-type ESCs, PGCLCs, or *Mad2l2*-deficient ESCs transfected with a *Mad2l2-GFP* vector. MAD2L2 derepresses the *Dppa3* promoter by blocking EHMT1/2 and, thus, the formation of H3K9me2. The high level of DPPA3 displaces DNMT1 from UHRF1, and thus prevents methylation of the new DNA strand.

Cell Fractionation

Three independent biological replicates were prepared from 10^8 cells each, and were fractionated into cytoplasmic, nucleoplasmic, and chromatin fractions. See Supplemental Experimental Procedures for further details.

RT-PCR

At least three independent replicates, with two technical replicates each, were performed using the following primer pairs: Gapdh (5′-GTC GTG GAG TCT ACT GGT GTC-3′ and 5′-GAG CCC TTC CAC AAT GCC AAA-3′), Dppa3 (5′-CGT CCT ACA ACC AGA AAC AC-3′ and 5′-CTG CTC AAT CCG AAC AAG TC-3′), and Mad2l2 (5′-GTT GCC TTG AGT CCC TAC AG-3′ and 5′-TCC ACA TCG TTC TTC TCC AG-3′).

Immunocytochemistry

Immunocytochemistry was performed as specified in Supplemental Experimental Procedures. Sections were analyzed by confocal or stimulated emission depletion microscopy.

ChIP-Seq and MeDIP-Seq

ChIP was performed for three independent replicates as described in Supplemental Experimental Procedures (Adli and Bernstein, 2011).

RNA-Seq

Previously reported fastq files (Pirouz et al., 2015) were re-evaluated as specified in the Supplemental Experimental Procedures.

Dot Blot

Dot-blot analysis was performed as described by Hayashi et al. (2011). Three independent replicates of 50 ng DNA were applied to a membrane filter, and the methylation level was detected with an antibody against 5mC (Abcam).

ACCESSION NUMBERS

Sequencing data are available from the European Nucleotide Archive under accession number ENA: PRJEB19344 at http://www.ebi.ac.uk/ena/data/view/PRJEB19344.

SUPPLEMENTAL INFORMATION

Supplemental Information includes Supplemental Experimental Procedures, four figures, and one movie and can be found with this article online at http://dx.doi.org/10.1016/j.stemcr.2017.02.011.

AUTHOR CONTRIBUTIONS

M.K. initiated, led, and managed the project, and wrote the paper. A.R. co-designed the study, performed the majority of experiments and the bioinformatics analyses, and contributed critically to text and figures. M.P. generated the Mad2l2-deficient ES line, and was involved in the early concept of the project. M.d.V. helped with interpretations. D.K. performed stimulated emission depletion microscopy.

ACKNOWLEDGMENTS

The work was supported by the Max Planck Society. M.D.V. is a Helmholtz Association young investigator. We thank M. Saitou (Kyoto University) and M. Boiani (MPI Muenster) for ESC lines, G. Salinas (Goettingen University) for sequencing, and H. Jäckle for his hospitality.

Received: August 30, 2016
Revised: February 13, 2017
Accepted: February 14, 2017
Published: March 16, 2017

REFERENCES

Adli, M., and Bernstein, B.E. (2011). Whole-genome chromatin profiling from limited numbers of cells using nano-ChIP-seq. Nat. Protoc. *6*, 1656–1668.

Banath, J.P., Banuelos, C.A., Klokov, D., MacPhail, S.M., Lansdorp, P.M., and Olive, P.L. (2009). Explanation for excessive DNA single-strand breaks and endogenous repair foci in pluripotent mouse embryonic stem cells. Exp. Cell Res. *315*, 1505–1520.

Boersma, V., Moatti, N., Segura-Bayona, S., Peuscher, M.H., van der Torre, J., Wevers, B.A., Orthwein, A., Durocher, D., and Jacobs, J.J. (2015). MAD2L2 controls DNA repair at telomeres and DNA breaks by inhibiting 5′ end resection. Nature *521*, 537–540.

Bortvin, A., Goodheart, M., Liao, M., and Page, D.C. (2004). Dppa3/Pgc7/stella is a maternal factor and is not required for germ cell specification in mice. BMC Dev. Biol. *4*, 2.

Esteve, P.O., Chin, H.G., Smallwood, A., Feehery, G.R., Gangisetty, O., Karpf, A.R., Carey, M.F., and Pradhan, S. (2006). Direct interaction between DNMT1 and G9a coordinates DNA and histone methylation during replication. Genes Dev. *20*, 3089–3103.

Funaki, S., Nakamura, T., Nakatani, T., Umehara, H., Nakashima, H., and Nakano, T. (2014). Inhibition of maintenance DNA methylation by Stella. Biochem. Biophys. Res. Commun. *453*, 455–460.

Gaspar-Maia, A., Alajem, A., Meshorer, E., and Ramalho-Santos, M. (2011). Open chromatin in pluripotency and reprogramming. Nat. Rev. Mol. Cell Biol. *12*, 36–47.

Habibi, E., Brinkman, A.B., Arand, J., Kroeze, L.I., Kerstens, H.H., Matarese, F., Lepikhov, K., Gut, M., Brun-Heath, I., Hubner, N.C., et al. (2013). Whole-genome bisulfite sequencing of two distinct interconvertible DNA methylomes of mouse embryonic stem cells. Cell Stem Cell *13*, 360–369.

Hayashi, K., Lopes, S.M., Tang, F., and Surani, M.A. (2008). Dynamic equilibrium and heterogeneity of mouse pluripotent stem cells with distinct functional and epigenetic states. Cell Stem Cell *3*, 391–401.

Hayashi, K., Ohta, H., Kurimoto, K., Aramaki, S., and Saitou, M. (2011). Reconstitution of the mouse germ cell specification pathway in culture by pluripotent stem cells. Cell *146*, 519–532.

Kang, J., Kalantry, S., and Rao, A. (2013). PGC7, H3K9me2 and Tet3: regulators of DNA methylation in zygotes. Cell Res. *23*, 6–9.

Liu, X., Gao, Q., Li, P., Zhao, Q., Zhang, J., Li, J., Koseki, H., and Wong, J. (2013). UHRF1 targets DNMT1 for DNA methylation

through cooperative binding of hemi-methylated DNA and methylated H3K9. Nat. Commun. *4*, 1563.

Magnusdottir, E., Dietmann, S., Murakami, K., Gunesdogan, U., Tang, F., Bao, S., Diamanti, E., Lao, K., Gottgens, B., and Azim Surani, M. (2013). A tripartite transcription factor network regulates primordial germ cell specification in mice. Nat. Cell Biol. *15*, 905–915.

Meshorer, E., and Misteli, T. (2006). Chromatin in pluripotent embryonic stem cells and differentiation. Nat. Rev. Mol. Cell Biol. *7*, 540–546.

Nakamura, T., Arai, Y., Umehara, H., Masuhara, M., Kimura, T., Taniguchi, H., Sekimoto, T., Ikawa, M., Yoneda, Y., Okabe, M., et al. (2007). PGC7/Stella protects against DNA demethylation in early embryogenesis. Nat. Cell Biol. *9*, 64–71.

Noon, A.T., Shibata, A., Rief, N., Lobrich, M., Stewart, G.S., Jeggo, P.A., and Goodarzi, A.A. (2010). 53BP1-dependent robust localized KAP-1 phosphorylation is essential for heterochromatic DNA double-strand break repair. Nat. Cell Biol. *12*, 177–184.

Ohinata, Y., Sano, M., Shigeta, M., Yamanaka, K., and Saitou, M. (2008). A comprehensive, non-invasive visualization of primordial germ cell development in mice by the Prdm1-mVenus and Dppa3-ECFP double transgenic reporter. Reproduction *136*, 503–514.

Payer, B., Saitou, M., Barton, S.C., Thresher, R., Dixon, J.P., Zahn, D., Colledge, W.H., Carlton, M.B., Nakano, T., and Surani, M.A. (2003). Stella is a maternal effect gene required for normal early development in mice. Curr. Biol. *13*, 2110–2117.

Pirouz, M., Pilarski, S., and Kessel, M. (2013). A critical function of Mad2l2 in primordial germ cell development of mice. PLoS Genet. *9*, e1003712.

Pirouz, M., Rahjouei, A., Shamsi, F., Eckermann, K.N., Salinas-Riester, G., Pommerenke, C., and Kessel, M. (2015). Destabilization of pluripotency in the absence of Mad2l2. Cell Cycle *14*, 1596–1610.

Rothbart, S.B., Krajewski, K., Nady, N., Tempel, W., Xue, S., Badeaux, A.I., Barsyte-Lovejoy, D., Martinez, J.Y., Bedford, M.T., Fuchs, S.M., et al. (2012). Association of UHRF1 with methylated H3K9 directs the maintenance of DNA methylation. Nat. Struct. Mol. Biol. *19*, 1155–1160.

Shinkai, Y., and Tachibana, M. (2011). H3K9 methyltransferase G9a and the related molecule GLP. Genes Dev. *25*, 781–788.

Singer, Z.S., Yong, J., Tischler, J., Hackett, J.A., Altinok, A., Surani, M.A., Cai, L., and Elowitz, M.B. (2014). Dynamic heterogeneity and DNA methylation in embryonic stem cells. Mol. Cell *55*, 319–331.

Turinetto, V., Orlando, L., Sanchez-Ripoll, Y., Kumpfmueller, B., Storm, M.P., Porcedda, P., Minieri, V., Saviozzi, S., Accomasso, L., Cibrario Rocchietti, E., et al. (2012). High basal gammaH2AX levels sustain self-renewal of mouse embryonic and induced pluripotent stem cells. Stem Cells *30*, 1414–1423.

Willig, K.I., Rizzoli, S.O., Westphal, V., Jahn, R., and Hell, S.W. (2006). STED microscopy reveals that synaptotagmin remains clustered after synaptic vesicle exocytosis. Nature *440*, 935–939.

Xu, G., Chapman, J.R., Brandsma, I., Yuan, J., Mistrik, M., Bouwman, P., Bartkova, J., Gogola, E., Warmerdam, D., Barazas, M., et al. (2015a). REV7 counteracts DNA double-strand break resection and affects PARP inhibition. Nature *521*, 541–544.

Xu, X., Smorag, L., Nakamura, T., Kimura, T., Dressel, R., Fitzner, A., Tan, X., Linke, M., Zechner, U., Engel, W., et al. (2015b). Dppa3 expression is critical for generation of fully reprogrammed iPS cells and maintenance of Dlk1-Dio3 imprinting. Nat. Commun. *6*, 6008.

Ying, Q.L., Wray, J., Nichols, J., Batlle-Morera, L., Doble, B., Woodgett, J., Cohen, P., and Smith, A. (2008). The ground state of embryonic stem cell self-renewal. Nature *453*, 519–523.

Stem Cell Reports, Volume *8*

Supplemental Information

MAD2L2 Promotes Open Chromatin in Embryonic Stem Cells and Derepresses the *Dppa3* Locus

Ali Rahjouei, Mehdi Pirouz, Michela Di Virgilio, Dirk Kamin, and Michael Kessel

SUPPLEMENTAL INFORMATION

Supplemental Experimental Procedures

Cell culture.
Mad2l2-deficient ESCs carrying an Oct4-GFP ESCs have an insertion of the GFP open reading frame behind the Oct4 enhancers CR I, II and IV, while CR II is deleted (Boiani et al., 2004). GFP expression demarcates the early embryonic epiblast, PGCs, and ESCs, but not the late epiblast. In order to visualize Dppa3 expression we employed BVSC ESCs were generated and provided by M. Saitou (Kyoto University, Japan). ESCs were transfected with Lipofectamine 2000 as recommended, and 8 h after transfection cells were harvested (three independent biological replicates). MEFs were generated and grown as described (Pirouz et al., 2013). DNA damage was induced wit 50 nM mitomycin for 20 min. Histone acetylation was inhibited with Trichostatin A (SIGMA; 250 nM) or SAHA (SIGMA; 10 μm) for eight hours in LIF/2i medium (three independent biological replicates).

Flow cytometry.
Trypsinized cells were labelled with antibodies, washed, and then fixed in methanol (-20 °C). After washing they were resuspended in blocking solution (1% bovine serum albumin, 1% Tween, 22.52 mg/ml glycine in phosphate buffered saline (PBS). Antibodies were applied overnight at 4 °C. Slides were washed three times for 10 minutes with PBS. Secondary antibody was applied and incubated for 60 minutes at room temperature. Slides were washed three times for 10 minutes with PBS.

Cell fractionation.
10^8 cells were pelleted, washed and resuspended in 2 ml of ice-cold NP-40 lysis buffer. Nuclei were pelleted at 120 x g at 4 °C for 10 min, and the supernatant cytoplasmic fraction was saved. Pellet was resuspended in 1 ml low salt buffer + 1% Triton X-100 and incubated on ice for 10 min. Chromatin fraction was pelleted at 120 x *g* at 4 °C for 10 min, and the supernatant nucloplasmic fraction was saved. Chromatin fraction was solved in 125 μl of 0.2 N HCl and neutralized with same volume of Tris-HCl pH8.

Cryosectioning. PGCLC aggregates were harvested, washed, and fixed in 4% formaldehyde (pH 7.4) for 2 hours. Cells were dehydrated by transfer to 10%, 20% and 30% sucrose solutions. Finally, the aggregates were transferred into tissue-tek solution, and frozen on dry ice. Cryo-microtome sections were stored at -80 °C.

RT-PCR. RNA and cDNA were prepared by standard procedures, and amplifications were executed with a Biosystems 7300 Sequence Detection system. All experiments were repeated for at least three times independently, with two technical replicates each. Primers were designed by the primer-blast tools from NCBI. Expression levels were calculated based on Ct values after normalization for GAPDH.

Immunocytochemistry. Cells were cultured on chamber slides (Nuc Lab-Tek), washed with PBS, and rinsed with NP-40/0.2% PBS for 10 min for permeabilization. Washing steps were repeated by PBT. Cells were covered with blocking solution for 60 minutes (1% BSA, 22.52 mg/ml glycine in PBT). The first antibody was applied overnight at 4 °C, and after washing the secondary antibody was applied for 60 minutes. Slides were washed, and mounted in Mounting Medium with DAPI (Vector Laboratories). Samples were documented by confocal (Leica SP3) or Stimulated Emission Depletion (STED) microscopy. ImageJ software (https://imagej.nih.gov/ij/) was used for all image processing and quantifications.

The following primary antibodies were used at dilutions of 1:100 or 1:200: Anti-DPPA3 (Santa Cruz, sc-19878), Anti-H3K9me2 (Abcam, ab6002), Anti-H3K27me3 (Abcam, ab8580), Anti-RNF168 (Santa Cruz, sc-101125), Anti-53BP1 (Santa Cruz, sc-22760), MAD2l2 (Abcam, ab180579). Secondary antibodies were Alexa Fluor 488 (Thermo Fisher, Z25002, Z25302), Alexa Fluor 594 (Thermo Fisher, Z25007, Z25007), Alexa Fluor 647 (Thermo Fisher, Z25308), STAR 635 and STAR 580 (Abberior, Goettingen, 2-0032-051-9).

STED microscopy. The procedure was modified from (Revelo et al., 2014). Immunostained cells were transferred to unpolymerized resin *(p*-toluenesulfonic acid monohydrate/2,4,6-Tris[bis(methoxymethyl)amino]-1,3,5-triazine) in a BEEM capsule. Samples were kept overnight at room temperature to allow penetration of melamine, and were then warmed to 40°C for 24 h. The BEEM capsule was filled to the top with Epon resin (EpoFix kit; Struers), and heated to 60°C for 48 h. Ultrathin sections of 30 or 80 nm were prepared with an ultramicrotome (EM UC6; Leica) and documented by high resolution STED microscopy (TCS SP5; Leica).

ChIP-seq and MeDIP-seq. DNA libraries were produced with the QuantiFluor dsDNA System (Promega), and the size range was determined with the Bioanalyzer 2100 (Agilent). Libraries were amplified and sequenced at 100 bp resolution with an
Illumina HiSeq2000 sequencer. The Illumina software BaseCaller was used for the conversion of sequence images to Fastq files, which were analyzed for quality with the fastx_toolkit. Alignment was performed with bowtie 2 software for Illumina based on the mm10 reference genome. Duplications were removed with RmDup (version 2.0.0). The reference genome was annotated by merging with a Gff3 file. Merged files in combination with the INPUT file were used for peak calling by MACS (version 2.2.2). Methylated areas were recognized by the MEDIPS package of the R software (version 3.2.2) (Weber et al., 2005). Data were visualized by Integrative Genomics Viewer (version 2.3).

RNAseq. Previously reported fastq files (Pirouz et al., 2015) were re-evaluated by alignment with BWA for Illumina, based on mm10 instead of mm9. BAM files were prepared with a procedure similar to ChIP-seq data. Significant changes of gene expression were determined by the two independent methods Cuffdiff and deseq2. Data were visualized by the Visualization-Bioconductor package of the R software.

Supplemental References

Boiani, M., Kehler, J., and Scholer, H.R. (2004). Activity of the germline-specific Oct4-GFP transgene in normal and clone mouse embryos. Methods Mol Biol *254*, 1-34.

Hayashi, K., Ohta, H., Kurimoto, K., Aramaki, S., and Saitou, M. (2011). Reconstitution of the mouse germ cell specification pathway in culture by pluripotent stem cells. Cell *146*, 519-532.

Pirouz, M., Pilarski, S., and Kessel, M. (2013). A critical function of Mad2l2 in primordial germ cell development of mice. PLoS Genet *9*, e1003712.

Pirouz, M., Rahjouei, A., Shamsi, F., Eckermann, K.N., Salinas-Riester, G., Pommerenke, C., and Kessel, M. (2015). Destabilization of pluripotency in the absence of Mad2l2. Cell Cycle *14*, 1596-1610.

Revelo, N.H., Kamin, D., Truckenbrodt, S., Wong, A.B., Reuter-Jessen, K., Reisinger, E., Moser, T., and Rizzoli, S.O. (2014). A new probe for super-resolution imaging of membranes elucidates trafficking pathways. J Cell Biol *205*, 591-606.

Weber, M., Davies, J.J., Wittig, D., Oakeley, E.J., Haase, M., Lam, W.L., and Schubeler, D. (2005). Chromosome-wide and promoter-specific analyses identify sites of differential DNA methylation in normal and transformed human cells. Nat Genet *37*, 853-862.

Supplemental Figures

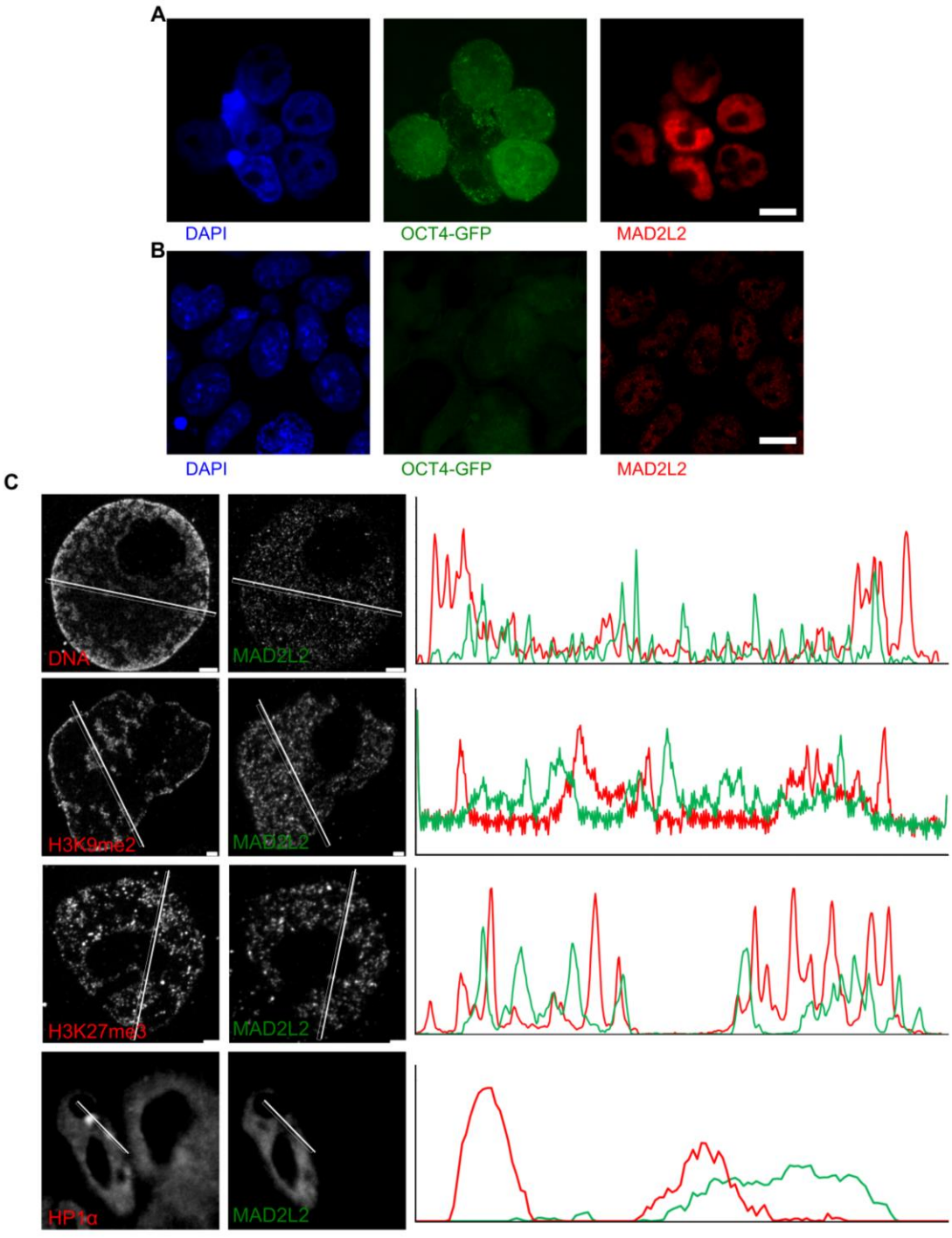

Figure S1 (Related to Figure 1). Downregulation of MAD2L2 Accompanies The Transition from Naive to Primed Pluripotency

(A) High levels of MAD2L2 protein in naive ESCs grown in LIF/2i medium, note heterogeneity of MAD2L2, but not Oct4-GFP expression.

(B) Absence of MAD2L2 protein from EpiLCs, which were generated from ESCs by growth in medium containing activin, bFGF and serum replacement for 6 days. Magnification bars (A,B) = 10 µm. All observations in Figure S1A,B, were confirmed with three experimental replicates.

(C) Line scan histogram profiles through Figure 1B,C,E demonstrate that MAD2L2 protein (green profiles) does not colocalize with compact DNA, and the heterochromatin markers H3K9me2, H3K27me3 and HP1alpha (red profiles).

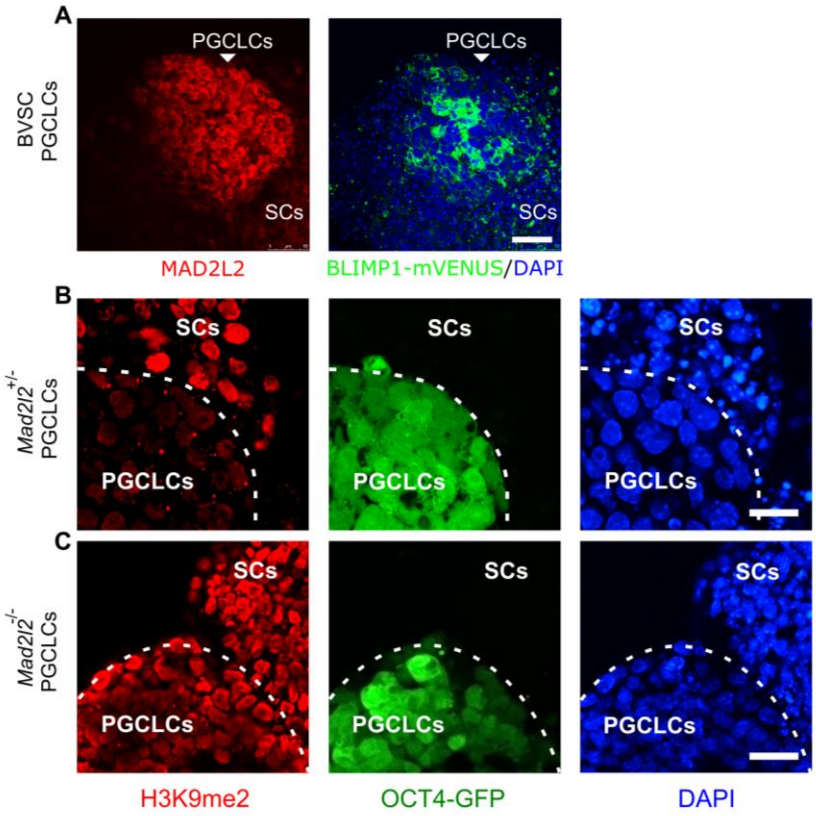

Figure S2 (Related to Figure 3). *Mad2l2*-deficient PGCLCs Do Not Switch Their Histone 3 modifications

(A) MAD2L2 expression in wild-type PGCLCs, which were identified by expression of a BLIMP1-mVenus transgene (Hayashi et al., 2011).

(B) Wild-type PGCLCs identified by an Oct4-GFP transgene have lost the expression of H3K9me2, while *Mad2l2*-deficient PGCLCs maintained high levels. H3K9me2 expression in GFP-negative, somatic cells (SCs) was not affected by the *Mad2l2* mutation.

Magnification bars = 50 μm (A), = 25 μm(B).

All observations were confirmed with three experimental replicates.

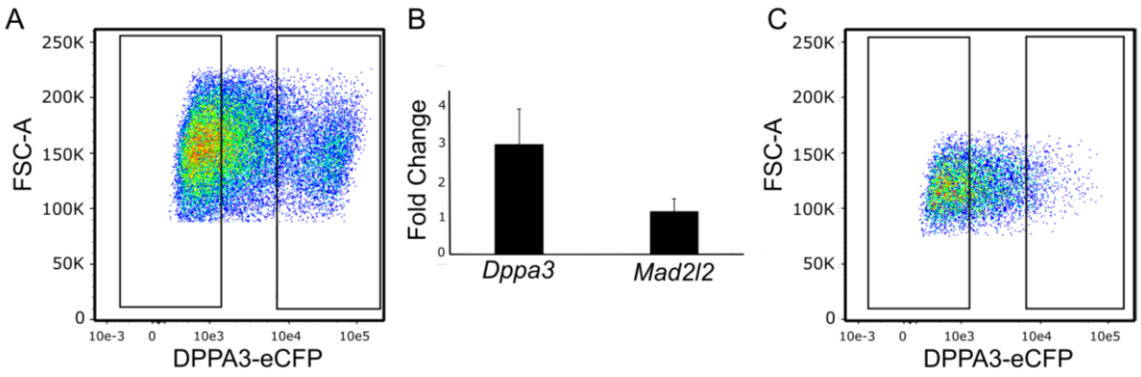

Figure S3 (Related to Figure 3). Recovery of Dppa3 and Mad2l2 expression

(A) BVSC-ESCs grown in LIF/2i medium were sorted into two populations based on the high or low expression of the *Dppa3-eCFP* transgene.

(B) In both populations the expression of *Dppa3* and *Mad2l2* were determined by qPCR. For each value, the average numbers from three independent experiments were calculated. These data confirm a positive correlation between *Mad2l2* and *Dppa3* expression. Standard deviations were calculated based on three experimental replicates.

(C) DPPA3-eCFP-negative ESCs were recultured for 24 hours in LIF/2i. FACS analysis revealed that a fraction of cells had re-established expression of the DPPA3-eCFP transgene. These data suggest that also *Mad2l2* expression was recovered.

To separate negative and positive cells, two gates were placed based on a control negative cell line to the far left side for the negative cells and to the area in the right site with zero cell population for the positive cells.

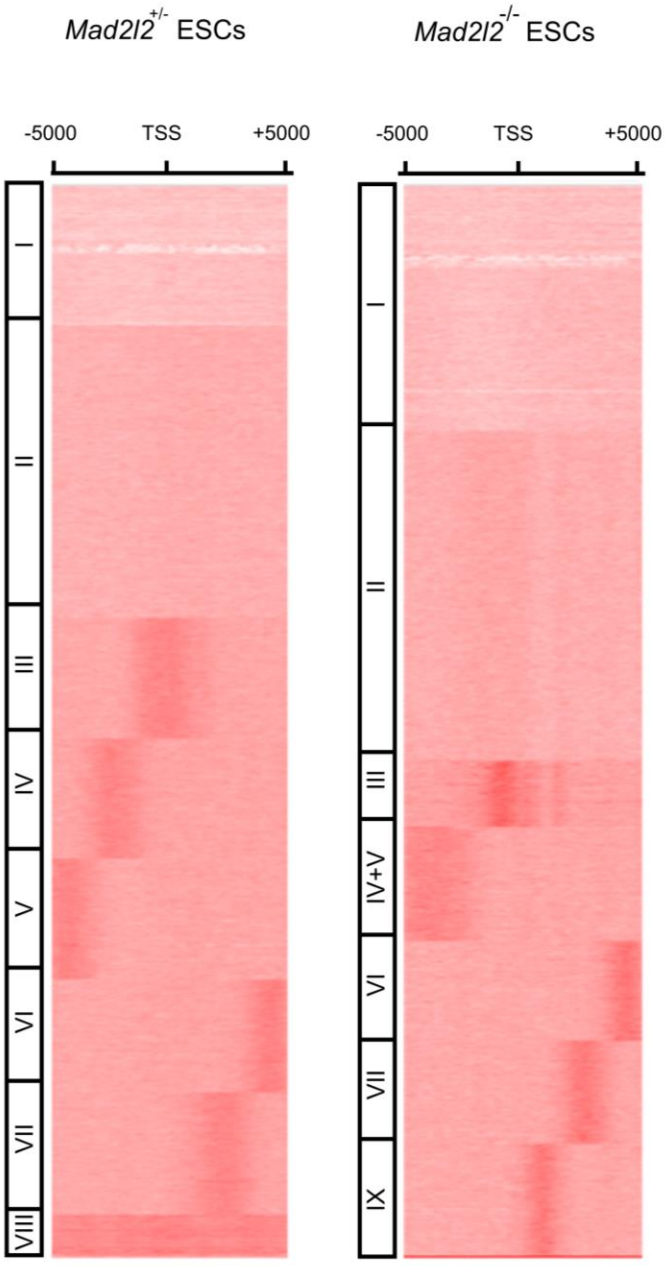

Figure S4 (Related to Figure 4). Perturbed Methylation Patterns Around the Transcriptional Start Sites in The Genome of Mutant ESCs

The distribution of 5mC between position -5000 bp and +5000 bp around the transcription start site were evaluated for 65.000 transcripts. Methylated regions were classified based on their distance from the transcription start sites. In Figure 4C the scans of class III regions for wild-type and *Mad2l2*-deficient ESCs are depicted. This observation was confirmed with three experimental replicates.

Legend for Supplemental Movie S1 (Related to Figure 1A)

The movie shows a 3D laser scan of MAD2L2 expression in one ESCs colony by confocal microscopy. Note that the antibody staining is on peripheral as well as internal cells, demonstrating that equal staining was obtained, and differences are not due to accessibility and penetration.